Multifractal structure and Gutenberg-Richter parameter associated with volcanic emissions of high energy in Colima, México (years 2013-2015)

Marisol Monterrubio-Velasco[1], Xavier Lana[2], Raul Arámbula-Mendoza[3]

[1] Department of Computer Applications of Science and Engineering, Barcelona Supercomputing Center, 08034, Barcelona, Spain

[2] Department of Physics, ETSEIB, Universitat Politècnica de Catalunya, Diagonal 647, 08028 Barcelona, Spain

[3] Centro Universitario de Estudios e Investigaciones de Vulcanología (CUEIV), Universidad de Colima, Colima, 28045, México

Abstract

The evolution of multifractal structures in various physical processes, such as climatology, seismology, or volcanology, serves as a crucial tool for detecting changes in corresponding phenomena. In this study, we explore the evolution of the multifractal structure of volcanic emissions with varying energy levels (observed at Colima, México, during the years 2013-2015) to identify clear indicators of imminent high-energy emissions nearing 8.0×10^8 J. These indicators manifest through the evolution of six multifractal parameters: the central Hölder exponent (α_0), maximum and minimum Hölder exponents (α_{max}, α_{min}), multifractal amplitude ($W = \alpha_{max} - \alpha_{min}$), multifractal asymmetry ($\gamma = [\alpha_{max} - \alpha_0]/[\alpha_0 - \alpha_{min}]$), and the complexity index (CI), calculated as the sum of normalized values of α_0, W and γ. Additionally, the results obtained from adapting the Gutenberg-Richter seismic law to volcanic energy emissions, along with the corresponding skewness and standard deviation of the volcanic emission data, further support the findings obtained through multifractal analysis. These results, derived from multifractal structure analysis, adaptation of the Gutenberg-Richter law to volcanic emissions, and basic statistical parameters, hold significant relevance in anticipating potential volcanic episodes of high energy. Such anticipation can be further quantified using an appropriate forecasting algorithm.

Key-words: volcanic emissions, Colima (México), extreme energy emission, multifractal structure, Gutenberg-Richter parameter evolution.

1 Introduction

The application of fractal and multifractal theory to Earth sciences (Goltz, 1997; Turcotte, 1997; Karsten et al., 2005, among others) represents an intriguing avenue for analysing complex geophysical and atmospheric phenomena, serving as a significant step in the forecasting process. Examples include studying rainfall patterns (Koscielny-Bunde et al., 2006; Lana et al., 2017, 2020, 2023), extreme temperature variations (Burgueño et al., 2014), wind speed characteristics (Feng, 2009), hydrological analysis (Movahed M. S. and Hermanis E., 2008), seismic activity (Gosh et al., al., and 2012; Telesca and Toth, 2016 and Monterrubio-Velasco et al., 2020) and emissions of volcanic energy (Monterrubio-Velasco et al., 2023).

The forecasting of volcanic energy emissions through the monofractal theory, specifically the Hurst exponent and Reconstruction theorem (Diks, 1999), along with predictive algorithms and nowcasting processes (Rundle et al., 2016), could play a crucial role in averting imminent hazardous events. One application of monofractal theory can be seen in the analysis of volcanic emission data from Colima, México, spanning the years 2013 to 2015 (Arámbula-Mendoza et al., 2018, 2019; Monterrubio-Velasco et al., 2023). This analysis, in conjunction with nowcasting, helps to predict the probable energy levels of upcoming emissions. In contrast, a different approach is rooted in multifractal theory (Kantelhardt et al., 2002), which has also been employed in fields such as seismology (Shadkhoo and Jafari, 2009; Telesca and Toth, 2016) and climatology (Mali, 2014; Lana et al., 2016, 2017). This theory offers an alternative perspective and methodology for understanding complex systems and their behaviours across various scientific domains.

One of the most relevant laws in seismology, the Gutenberg-Richter equation (Gutenberg and Richter, 1944; Aki, 1981; Amitrano, 2003; Scholz, 2015; Zaccagnino and Doglioni, 2022) describes the earthquake frequency-magnitude distribution for local, regional, or global seismic sequences:

$$\log_{10}\left[N \geq M_w\right] = a - b\left(M_w - M_c\right) \tag{1}$$

where N represents the cumulated number of events exceeding a magnitude M_w and the parameter b, usually called b-value, is associated with the scaling of the number earthquakes for increasing values of the seismic magnitude. The magnitude of completeness M_c, refers to the smallest earthquake magnitude that is consistently recorded within a given dataset or region. It represents the threshold above which all earthquakes are reliably detected and cataloged by a seismic network. This concept is crucial for ensuring the accuracy and reliability of statistical analyses and for making meaningful interpretations about seismic activity and earthquake distribution. The b-value is mainly controlled by: (1) the fractal distribution of seismic sources (Aki, 1981; Zaccagnino et al., 2022); (2) Fault roughness (Amitrano, 2023); (3) The b-value is also related to the differential stress of the Earth's crust: highly stressed zones, or faults, usually exhibit low b-values, whereas weakly stressed areas usually exhibit higher b-values (Scholz, 2015). Gulia and Wiemer, (2019) suggest that a decrease in b-value on the mainshock's fault can indicate that the strongest event of the sequence has not yet occurred, being this information useful to forecast future stronger earthquakes. For these reasons, analysing the time series of the b-value can be a powerful tool to enhance seismologist forecasting capability (Taroni et al., 2021). The Gutenberg-Richter equation is also useful for the analysis of volcanic emissions bearing in mind the seismic moment magnitude, M_w, is related to the emission of seismic energy, E_s, by means of the power law (Kanamori, 1977)

$$M_w = 2/3 \log_{10} E_s - 3.2 \tag{2}$$

Hence, it is feasible to utilize an equivalent Gutenberg-Richter law in the current study, replacing seismic magnitudes with the logarithm of volcanic energy emissions (E) in the series of volcanic explosions at Volcán de Colima:

$$\log_{10} N = -b \log_{10} E + a \tag{3}$$

The objective of this research is not forecasting the magnitude of the next emission but verifying that a specific evolution of a set of multifractal parameters, based on the successive analysis of data series, could manifest the vicinity of a future real extreme

energetic emission. It is also relevant that the results obtained from the viewpoint of the multifractality agree with the evolution of the *b*-value when the segments of volcanic emissions are approaching to the extreme emission of energy.

The second section, Database, details the basic characteristics of the complete set of emissions and justifies the database quality. The third section, Multifractal Theory, is divided into three parts, corresponding to, first, a detailed description of the multifractal detrended fluctuation theory, second, the multifractal spectrum and, third, the complexity index. The fourth section, Evolution of the Multifractal Parameters, depicts the use of characteristics of all the multifractal parameters for detecting the vicinity to an extreme emission of volcanic energy. Additionally, the Gutenberg-Richter evolution confirms the vicinity of an extreme emission of energy by means of changes on the *b*-value. The fifth section provides a summary of the obtained results, along with a discussion on the effectiveness of this strategy and its comparison with forecasting and nowcasting processes.

2 Database

Series of volcanic explosions, also known as Vulcanian episodes (Bachtell Clarke and Esposti Ongaro, 2015), emitted by Volcán de Colima (Western segment of Trans-Mexican volcanic belt) along years 2013-2015 (Arámbula-Mendoza et al., 2018, 2019) have been chosen to analyse, from the point of view of the multifractal theory, the imminence of emissions associated with energies close to or exceeding 10^8 Joules.

Figure 1 illustrates the emissions conforming to the Gutenberg-Richter law, as outlined before, comprising a dataset of 6182 instances where the energy is equal to or exceeds approximately 2×10^6 J within the frame time of years 2013-2015. The most relevant energy emissions are detected just at the beginning of the recorded data [$\log_{10}$ (Energy) =8.2], approximately at the middle of the series [$\log_{10}$(Energy) = 8.4] and at the end of the series [$\log_{10}$(Energy) = 8.9]. Monterrubio-Velasco et al. (2023) develops a more complete statistical description of volcanic emissions, using the Generalized Logistic Distribution (GLO) in the framework of the L-moment theory (Hosking and Wallis, 1997). This study includes anticipated values for return periods associated with extreme emissions, characterized by probabilities of 90%, 95% and 99%, determined by the Generalized Extreme Values (GEV) distribution, also based on the L-moment distribution. Particularly, Monterrubio-Velasco et al. (2023) reveal that the highest extreme emissions, with a 90% probability, exceed an energy threshold corresponding to $\log_{10}$ (Energy) = 8.0.

As mentioned, two of the three maximum emissions are detected at the beginning and at the end of the dataset, being not possible to respectively complete the evolution of the multifractal parameters before and after these two extreme emissions. The research is finally applied to the emission of [$\log_{10}$(Energy) 8.4] with a detailed analysis applied to successive moving windows with a length of 1000 data (sufficient in this research for a right multifractality analysis) and a shift of 100 data, being obtained in this way 27 samples of the evolution of the different parameters describing the proximity to the highest emission. Figure 2a illustrates the progression of energy from emission 1500 to 3000, with the minimum, average, and maximum energy emissions corresponding to $\log_{10}$(Energy) values of approximately 6.3, 6.6, and 8.4, respectively (from the viewpoint of the TNT units, these energy emissions range from 0.4 to 67.4 kilograms of TNT). Consequently, the maximum energy emission surpasses the average energy of this segment by more than a hundredfold. The evolution of the energy from emission number

4

1500 (2013/12/10) up to emission number 3000 (2015/04/24) is also described in the Figure 2b, where are observed an evident reduction of the volcanic activity along 90- 100 consecutive days, previously to new activities close to the highest emission of energy.

3 Multifractal methodology

3.1 Multifractal Detrended Fluctuation Anaysis (MF-DFA)

The examination of multifractal characteristics in nonstationary series can be addressed by utilizing the multifractal detrended fluctuation analysis (MF-DF) technique, pioneered by Talkner and Weber (2000). A comprehensive description of the MF-DF methodology can be found in Kantelhardt et al. (2002). The MF-DF methodology is summarized below.

Considering $\{x_k\}$ as a time series with a length of N, the algorithm's steps are:

a) Computing the profile of the time series as

$$Y(i)=\sum_{k=1}^{i} x_k - \langle x \rangle, i=1,\ldots,N$$

(4)   where $< x >$ is the average value of the $\{x_k\}$.

b) Dividing *Y(i)* into N_s = *int(N/s)* non-overlapping segments of equal length *s*. Considering that the length *N* of the series is often not a multiple of the considered segment lengths, a short part at the end of the profile would be discarded. With the aim of not disregarding this part of the series, the same procedure is repeated starting from the opposite end. Consequently, $2N_s$ segments are obtained.

c) Computing the local variance $F^2(s,v)$ for each segment *v* of length s by using a n-order least-square polynomial fitting to obtain the differences between "profile" segments (first step) and the corresponding polynomial fitting. The degree of order of the polynomial is selected considering the best justified multifractal results. A fourth order degree is appropriate in our case.

d) Calculating the q-order fluctuation function:

$$F(s)_q=\left[\frac{1}{2N_s}\sum_{1}^{2N_s} \ln\left(F^2(s,v)\right)^{q/2}\right]^{1/qv} ,q\neq 0\,;-\infty<q<+\infty \tag{5}$$

$$F(s)_0=\left[\frac{1}{4N_s}\sum_{1}^{2N_s} \ln\left(F^2(s,v)\right)\right],q=0 \tag{6}$$

The steps b, c and d must be repeated for several scales *s,* being appropriate that these scales vary within the range (*m+2, N/4*), where m =4 the chosen polynomial order (third step).

e) The q-order fluctuation function depicts a power-law relationship concerning the segment length, *s*:

$$F(s)_q \approx s^{h(q)} \tag{7}$$

and *h(q)*, the generalized Hurst exponent, can be determined by a linear regression of ln$\{F(S)_q\}$ versus ln*(s)*.

In the case of non-stationary series, such as fractal Brownian signals, the exponent $h(q = 2)$ will be larger than 1.0 and will satisfy $h(2) = H + 1$, where H is the well-known Hurst exponent (Movahed and Hermanis, 2008). For stationary time series, the value $h(q = 2)$ is identical to the Hurst exponent. $H > 0.5$ indicates persistence in long-range correlation, H 0.5 manifests the random character of the series, while $H < 0.5$ reflects anti-persistence. In the case of multifractal series, if positive values of q are considered, the segments ν with large variance (i.e. large deviations from the corresponding polynomial fit) will dominate the *Fq(s)* average. Thus, for positive values of q, $h(q)$ corresponds to the scaling behavior of the segments with large fluctuations. For negative values of q, the segments ν with small variance $F^2(s,\nu)$ will dominate the *Fq(s)* average, $h(q)$ then describing the scaling behavior of the segments with small fluctuations (Movahed and Hermanis, 2008; Burgueño et al., 2014).

3.2 The Singularity Spectrum

The singularity spectrum, f(α), is related to the generalized Hurst exponent h(q) through of the Legendre transform (Kantelhardt et al., 2002). This relationship is articulated as follows:

$$\alpha = h(q) + q \frac{dh(q)}{dq} \leftarrow LegendreTransfrom \rightarrow f(\alpha) = q[\alpha - h(q)] + 1 \tag{8}$$

where α is the Hölder exponent, which is used to study the scaling properties and the distribution of singularities. Each value of α corresponds to a different type of singularity, and the function of these exponents, known as the singularity spectrum $f(\alpha)$, describes the fractal dimension of the sets of points sharing the same Hölder exponent (Frish and Parisi, 1985; Lux, 2004). The multifractal scaling exponent also is known as mass exponent:

$$\tau(q) = qh(q) - 1 \tag{9}$$

and the Hölder exponent is defined as

$$\alpha(q) = d\tau(q)/dq \tag{10}$$

The function $f(\alpha)$ describes the subset dimension of the series characterized by the same singularity strength α, with the singularity strength with maximum spectrum designed as α_0. Small values of α_0 mean that the underlying process loses fine-structure, that is, becomes more regular in appearance; conversely, a large value of α_0 ensures higher complexity. The shape of $f(\alpha)$ may be fitted to a quadratic function around the position α_0:

$$f(\alpha) = A(\alpha - \alpha_0)^2 + B(\alpha - \alpha_0) + C \tag{11}$$

The coefficient B manifests the asymmetry of the spectrum, being null for a symmetric spectrum. A right-skewed spectrum, $B > 0$, indicates fine structure, while left-skewed shapes, $B < 0$, point to smooth structure. The width of the spectrum, W, can be obtained by extrapolating the fitted curve $f(\alpha)$ to zero or, in other words, extrapolating the multifractal spectrum to $q \rightarrow \pm\infty$. The spectral amplitude is defined as

$$W = \alpha_{max} - \alpha_{min} \tag{12}$$

210 with $f(\alpha_{max}) = f(\alpha_{min}) = 0$ and $\alpha_{max}(q \to -\infty)$ being larger than $\alpha_{min}(q \to +\infty)$. Given that q uses to be chosen many times ranging, for instance, within the (-15, +15) interval, α_{max} and α_{min} have been obtained by numerically extrapolating the Eq. (11) to $f(\alpha) = 0$.

The multifractal parameters used to detect the evolution towards an extreme energy emission are the central Hölder α_0, and the extreme Hölder exponents, α_{max} and α_{min},
215 respectively accomplishing $f(\alpha_0) = 1.0$ and $f(\alpha_{max}) = f(\alpha_{min}) = 0$. The multi-spectral amplitude W (Eq. 12) and the multifractal asymmetry γ,

$$\gamma = \frac{\alpha_{max} - \alpha_0}{\alpha_0 - \alpha_{min}} \tag{13}$$

also contribute to detect the vicinity of an extreme emission. All these parameters are combined in a single complexity index, CI, defined in Shimizu et al. (2002):

220 $$CI(j) = \left[\frac{\alpha_0(j) - \langle \alpha_0 \rangle}{\sigma(\alpha_0)} \right] + \left[\frac{W_j - \langle W \rangle}{\sigma(W)} \right] + \left[\frac{\gamma_j - \langle \gamma \rangle}{\sigma(\gamma)} \right] \tag{14}$$

with $j=1, ..., N$ representing the N data segments for which the multifractal spectrums is computed and $<*>$ and $\sigma(*)$, the corresponding average and standard deviation per each parameter calculated in the N samples. The evolution of every multifractal parameter close to the extreme emission of energy will be clearly decreasing or increasing
225 depending on every one of the specific parameters (α_0, α_{max}, α_{min}, W and γ), then affecting the global CI.

4. Results

4.1 Evolution of the multifractal parameters

The evolution of the multifractal parameters is analysed applying the multifractal
230 detrended fluctuation analysis algorithm, MF-DF, to 27 moving windows (MWs) data of length 1000 elements (sufficient to obtain accurate multifractal analyses, manifested by the obtained evolution of the Hölder exponent, the generalised Hurst exponent and a well obtained multifractal spectrum) and shift of 100 elements. In this way, the multifractal structure is analysed from the beginning of the available data series up to a
235 notable number of volcanic energy emissions after the onset of extreme energy E, which is close to $\log_{10}E = 8.4$. A first point of view of the evolution of the multifractal structure is depicted in Figure 3, where neither the first four moving windows (before the highest emission) nor the two last (after the highest emission) include the emission of the mentioned extreme energy. A simple review of the multifractal structure is not sufficient
240 to detect the vicinity to the highest emission, given that a good fit of the empiric values of multifractality to a theoretical 2nd degree polynomial structure does not imply vicinity to an extreme maximum emission. Nevertheless, the Hölder exponents, describing different multifractal amplitudes and asymmetries for every moving window suggest an alternative to detect the vicinity to the highest emission.

245 Fig. 4 describes the evolution of the Hölder parameter characteristics (α_0, α_{max}, α_{min}, W) for the 27 moving windows. Bearing in mind that the highest emission is included between the MW number 16 and 25, the most relevant results are:
    a) An increasing tendency of α_{max}, with some fluctuations before MW-15 and a clear decrease after the emission of the highest energy (MW-16).
250   b) Some fluctuation of α_{min}, up to MW-16 and a fast increase after this MW.

c) A clear decrease of α_0 arriving to MW-15, with a notable increase for some of the next MWs including the highest emission of energy.

d) A clear maximum of W for MW-16, together with evident increasing and decreasing evolutions, respectively before and after MW-16.

Additionally, Figure 5 depicts the evolution of the Hurst exponent, h(q=2), the multifractal asymmetry, γ, and the complexity index, CI. The corresponding characteristics are:

e) A quite similar structure of the Hurst exponent (h(q=2) in comparison with the evolution of α_0.

f) An evolution of the asymmetry γ quite similar like that corresponding to *W*.

g) An evolution of CI, also quite similar like that the evolution of W.

Another possibility for detection of the immediacy of a high energy emission is based on the evolution of the parameter $\tau(q) = qh(q) - 1$. Figure 6 depicts six examples of MWs (the first three not including the highest emission and the other three including it). As expected by the mathematical theory of the Multifractal algorithm, the change of the $d\tau(q)/dq$ is always detected in q = 0 and the corresponding square regression coefficients of both linear evolutions are very close to 1.0. Figure 7 describes the evolution of the two $d\tau(q)/dq$ for MWs numbers 9 to 19, where a quite evident diminishing of $d\tau(q)/dq$ for q>0 is noticeable up to MW16, including the moving window MW15 with the highest emission. Consequently, these results of the $d\tau(q)/dq$ for q>0 also contribute to detect the vicinity of the extreme volcanic emission by means of multifractal analyses.

The obtained good results for the multifractal structure of volcanic emissions of Colima (México), based on the fourth-order degree polynomials used, for instance, on cited seismology or climatology researches in this document, are also confirmed bearing in mind the well fitted empirical multifractal data to the theoretical multifractal scaling exponent,$\tau(q)$, and the theoretical singularity spectrum f(α).

4.2 Evolution of the Gutenberg-Richter *b*-value for volcanic emissions.

The results obtained by means of the multifractal theory are complemented by analysing the evolution of the b-value of the Gutenberg-Richter law adapted to volcanic emission of energy (Eq. 3), with the aim of detecting changes on this parameter along the 27 MWs.

The methodology we follow to measure the evolution of the *b*-value in the analyzed series is as follows:

1. **Determination of the Magnitude of Completeness (M_c)**: In this case, we calculate an analog of the magnitude of completeness using the entire $\log_{10}E$ series of volcanic emissions. M_c is determined by fitting the data to Equation 1 and calculating the coefficient of determination, ρ. The magnitude at which the coefficient of determination begins to decrease indicates the M_c. In our case the minimum acceptable $\log_{10}(E) = 6.3$ for every MW is also assumed to be the same obtained for the whole series of volcanic emissions (Fig. 1).

2. **Data Collection**: We gather 1000 consecutive energy emissions for each MW to ensure sufficient data for accurate analysis.

3. **Calculation of *b*-value**: Using Eq. 3, we compute the b-value for each MW, considering as M_c the computed in the first step. This involves considering the 1000 elements of each MW, measuring the frequency distribution of $\log_{10}E$, and fitting the data to Equation 3.

4. **Analysis of Trends and Abrupt Changes**: By examining the b-value evolution over time, we identify any significant deviations or abrupt changes in the series, which may indicate underlying shifts in the energy emissions.

The evolution of the b-value, together with standard deviation and skewness of the $\log_{10}E$ for the different MWs, is represented in Figs. 8a, 8b and 8c. Firstly, the decreasing trend of approximately 0.27 units of b for every MW from MW11 to MW16 is notable. Additionally, it is relevant that the b-values for the entire series (b=3.8, ρ=0.95), as shown in Fig. 1) and for MW16, the first Moving Window including the highest emission (b=4.2, ρ=0.96), are relatively similar. Additionally, the standard deviation of $\log_{10}E$ corresponding to MW16 (0.27) is also remarkable and like that corresponding to the whole series (0.28) and a clear increment of $\log_{10}E$ dispersion (standard deviation) is observed for the consecutive MWs approaching to the extreme emission. Something similar is detected for the skewness, with a value of 1.4 (the whole series) and of 1.3 (MW16), as well as a clear increment of the skewness approaching to the first MW including the extreme volcanic energy emission. In summary, considering the b-value evolution and two basic statistical measures (standard deviation and skewness), these three factors could together further confirm the progression toward a volcanic emission of extreme energy.

Despite the practicality offered by the multifractal parameters, the Gutenberg-Richter law and the standard deviation and skewness to detect possible forthcoming extreme emissions, the step-by-step forecasting of every emission (considering an appropriate algorithm and the results of the reconstruction theory) should be also relevant to complement the control of these emissions. On one hand, the results from this research illustrate that the evolution of various parameters clearly signals the occurrence of an extreme emission. On the other hand, a suitable forecasting algorithm could determine step by step, albeit with some level of uncertainty, the imminence of consecutive emissions. For example, an emission of $\log_{10}(E) = 7.52$, relatively close to the extreme one, is approximately recorded 17 days before. The other three high emissions {$\log_{10}(E)$ = 7.84, 7.71 and 7.65} are detected just a day or a few hours before the cited extreme emission. Remembering the foreshock concept in seismology, these four high emissions could be the "foreshocks" of the expected extreme emission. Nevertheless, whereas the first cited high emission, $\log_{10}(E) = 7.52$, could be a warning of 17 days before the extreme emission, the other three high emissions are detected only a few hours before the extreme episode. Conversely, the warning parameters proposed in this study detect signs of a forthcoming extreme energy emission a notable number of days before. A good example is the evolution of the Complexity Index, CI, which clearly increases since MW6 to MW11 (interval close to 100 days) and oscillates since MW12 to MW15 (close to 90 days before the extreme emission).

5. Conclusions

The analysis of the complexity and possible forecasting of potentially damaging volcanic emissions of energy, previously analysed from the point of view of the reconstruction theorem, have been now analysed in this study by means of the multifractal theory, with additional proxies based on the evolution of the b-value, and two basic statistical measures (standard deviation and skewness). The obtained results enable a deeper comprehension of the intricate physical mechanisms that govern these geophysical phenomena. It's essential not to overlook the significance of nowcasting, rooted in statistics, and forecasting algorithms, which rely on predictive models, and the reconstruction theorem. It's crucial to recall that the primary aim of this research is not

to provide precise forecasts for every volcanic energy emission. Rather, it focuses on identifying the most indicative parameters that exhibit trends suggestive of a potential onset of extreme energy emissions. In summary, the integration of multifractal structures theory, basic statistical parameters, and the Gutenberg-Richter law across a series of moving windows, together with the basis given by the reconstruction theorem, hold promise for significantly enhancing the predictability of high volcanic energy emissions over extended time intervals. Such advancements can aid preventively mitigating the effects of these volcanic emissions.

Competing interests

The contact author has declared that none of the authors has any competing interests.

Acknowledgment

References

Aki, K.: A probabilistic synthesis of precursory phenomena. Earthquake prediction. International Review, 4, 566-574. American Geophysical Union, Maurice Ewing series, D.W. Simpson and P.G. Richards, 1981. https://doi.org/10.1029/ME004p0566

Amitrano, D. Brittle-ductile transitions, and associated seismicity: experimental and numerical studies and relationship with the b value. Journal of Geophysical Research (Solid Earth), 108, B, 2003.
https://doi.org/10.1029/2001JB000680

Arámbula-Mendoza, R., Reyes-Dávila, G., Vargas-Bracamontes, D. M., González-Amezcua M., Navarro-Ochoa, C., Martínez-Fierros, A., Ramírez-Vázquez, A. Ariel.: Seismic monitoring of effusive-explosive activity and large lava dome collapses during 2013–2015 at Volcán de Colima, Mexico. Journal of Volcanology and Geothermal Research, 351, 75-88, 2018.

Arámbula-Mendoza, R., Reyes-Dávila, G., Domínguez-Reyes, T., Vargas-Bracamontes, D., González-Amezcua, M., Martínez-Fierros, A., Ramírez-Vázquez, A.: Seismic Activity Associated with Volcán de Colima. In Volcán de Colima, portrait of a Persistently Hazardous Volcano. Ed. Springer, 2019.

Bachtell Clarke, A., Esposti Ongaro, Belousov T.: Vulcanian eruptions. The Encyclopedia of Volcanoes, Editor in chief, Haraldur Sigurdsson. Elsevier, 2015.

Burgueño A., Lana X., Serra C., Martínez M.D.: Daily extreme temperature multifractals in Catalonia (NE Spain). Physics Letters A, 378, 874-885, 2014.

Diks, C.: Nonlinear time series analysis. Methods and Applications. Nonlinear Time Series and Chaos (4). World Scientific, 209 pp.10, 1999.

Feng T., Zuntao Fu Z., Deng X., Mao J. (2009): A brief description to different multi-fractal behaviours of daily wind speed records over China. Physics Letters A 373, 4134–4141.

Frisch U. and Parisi G. (1985): in Proceedings of the International School of Physics Enrico Fermi" Course 88: Turbulence and Predictability in Geophysical Fluid Dynamics and Climate Dynamics, North-Holland, New York.

390 Ghosh D., Dep A., Dutta S., Sengupta R., Samanta S.: Multifractality of radon concentration fluctuation in earthquake related signal. Fractals, 20, 33-39, 2012.

Goltz, Ch.: Fractal and chaotic properties of earthquakes. Lecture Notes in Earth Sciences (77), 178 pp, Springer-Verlag, Berlin, 1997.

Gulia, L. and Wiemer, S.: Real-time discrimination of earthquake foreshocks and
395 aftershocks. Nature, 574, 193–199, 2019. https://doi.org/10.1038/s41586-019-1606-4

Gutenberg, B. and Richter, C. Frequency of earthquakes in California. Bull. Seismol. Soc. Am. 34, 185–188, 1944.

Hosking, J.R.M. and Wallis, J.R.: Regional Frequency Analysis. An approach based on L-
400 Moments. Cambridge University Press, New York, 224 pp, 1997.

Kanamori, H.: The energy release in great earthquakes. Journal of Geophysical Research, 82 (20): 2981–2987, doi:10.1029/jb082i020p02981, 1977.

Kantelhardt J.W., Zschiegner S.A., Koscielny-Bunde E., Havlin S., Bunde A., Stanley H.E.: Multifractal detrended fluctuaction analysis of nonstationary time series. Physica A, 316,
405 87-114, 2002.

Karsten, B., Dimri, V.P., Maurizio, F.,Donato, F. Hiaso, I., Yasuto, K., La Manna, M., Lapenna, V., Pervukhina, M., Srivastava, H.N., Srivastava, R.P., Surkok, V.V., Tanaka, H., Telesca, L. Vedanti, N.: Fractal behaviour of the Earth system. Dimri, V.P. Editor. Springer-Verlag, 205 pp, 2005.

410 Koscielny-Bunde E., Kantelhardt J.W, Braund P., Bunde A., Havlin S.: Long-term persistence and multifractality of river runoff records: Detrended fluctuation studies. Journal of Hydrology 322,120–137, 2006.

Lana, X., Burgueño, A., Martínez, M.D., Serra, C.: Complexity and predictability of the monthly western Mediterranean oscillation index. International Journal of climatology, 36,
415 2435-2450, doi 10.1002/joc.4503, 2016.

Lana, X., Burgueño, A., Serra, C., Martínez, M.D.: Multifractality and autoregressive processes of dry spell lengths in Europe: an approach to their complexity and predictability. Theoretical and Applied Climatology, 127, 285-303. DOI 10.1007/s00704-015-1638-0, 2017.

420 Lana, X., Rodríguez-Solà, R., Martínez, M.D., Casas-Castillo, M. C., Serra, C., Kirchner,R.: Multifractal structure of the monthly rainfall regime in Catalonia (NE Spain): Evaluation of the non-linear structural complexity of the monthly rainfall. CHAOS: Interdisciplinary Journal of Nonlinear Science, 30(7). DOI: 10.1063/5.0010342, 2020.

Lana, X., Casas-Castillo, M.C., Rodríguez-Solà, R., Prohoms, M., Serra, C., Martínez, M.D.,
425 Kirchner, R.: Time trends, irregularity, multifractal structure and effects of CO_2 emissions on the monthly rainfall regime at Barcelona city, NE Spain, years 1786-2019. International Journal of Climatology, https://doi.org/10.1002/joc.7786, 2023.

11

Lux, T. (2004). Detecting multifractal properties in asset returns: the failure of the 'scaling estimator'. Int. J. mod. Phys. C,2004, 15, 481-491.

430 Monterrubio, M., Lana, X., Arámbula-Mendoza, R.: Uncertainties, complexities and possible forecasting of the volcán de Colima energy emissions (Mexico, years 2013-2015) based on the fractal reconstruction theorem. Nonlinear Process in Geophysics (In press). https://doi.org/10.5194/egusphere-2023-1153, 2023.

Mali P.: Multifractal characterization of global temperature anomalies.Theoretical and
435 Applied Climatology. DOI 10.1007/s00704-014-1268-y, 2014.

Monterrubio-Velasco, M., Lana, X., Martínez, M.D. Zúñiga, R. and de la Puente, J.: Evolution of the multifractal parameters along different steps of a seismic activity. The example of Canterbury 2000-2018 (New Zealand). AIP Advances. DOI: 10.1063/5.0010103, 2020.

440 Movahed M. S. and Hermanis E.: Fractal analysis of river flow fluctuations. Physica A, 387, 915–932, 2008.

Rundle, J.B., Turcotte, D.L., Donnellan, A., Grant, Ludwig, L., Luginbuhl, M., Gong, G.: Nowcasting earthquakes. AGU Publications. https://doi.org/10.1002/2016EA000185, 2016 .

445 Shadkhoo, S. and Jafari, G.R.: Multifractal Detrended Cross-Correlation Analysis of Temporal and Spatial Seismic Data. The European Physical Journal B, 72, 679-683, https://doi.org/10.1140/epjb/e2009-00402-2, 2009.

Shimizu Y., Thurner S., Ehrenberger K.: Multifractal spectra as a measure of complexity in human posture. Fractals, 10, 103-116, 2002.

450 Scholz, C.H.: On the stress dependence of the earthquake b value. Geophys. Res. Lett.. 42, 1399 –1402, 2015.
https://doi.org/10.1002/2014GL062863

Talkner, P., Weber, R.O.: Power spectrum and detrended fluctuation analysis: Application
455 to daily temperatures. Physical Review E 62, 150, 2000.

Taroni, M., Vocalelli, G., De Polis, A.: Gutenberg–Richter b-value Time Series Forecasting: A Weighted Likelihood Approach. Forecasting, 3, 561-569. https://doi.org/10.3390/forecast3030035, 2021.

Telesca, L. and Toth, L.: Multifractal detrended fluctuation analysis of Pannonian
460 earthquakes magnitude series. Physica A, 448, 21-29, 2016.

Turcotte, D.L.: Fractals and Chaos in Geology and Geophysics. Cambridge University press (2nd edition), 398 pp., 1997.

Zaccagnino, D., Doglioni, C. The impact of faulting complexity and type on earthquake rupture dynamics. Communications, Earth and Environment, 3, 258, 2022.
465 https://doi.org/10.1038/s43247-022-00593-5

470

The figure shows a plot with the y-axis labeled "N (CUMULATIVE EMISSIONS)" ranging from 1E+000 to 1E+005, and the x-axis labeled "Log(ENERGY), Joules" ranging from 3.0 to 9.0. The equation displayed is:
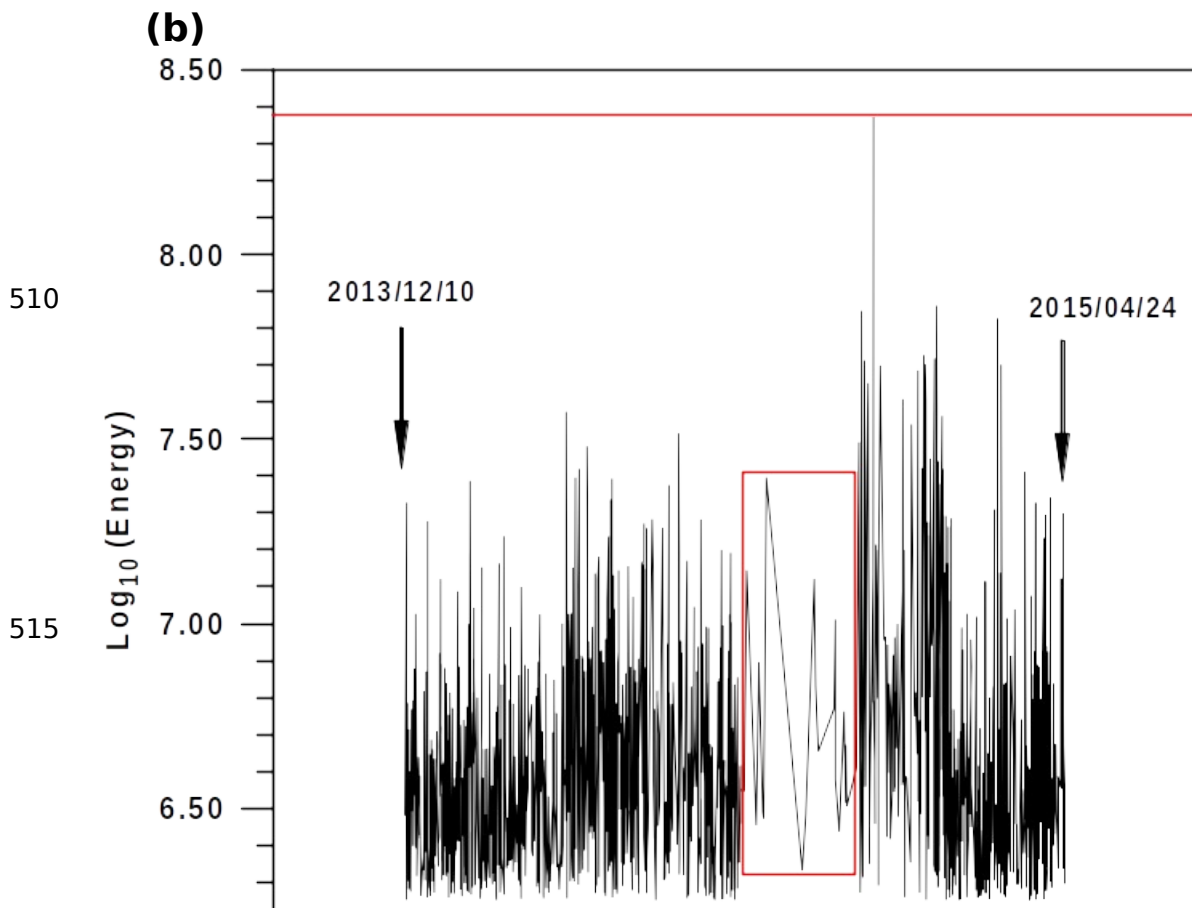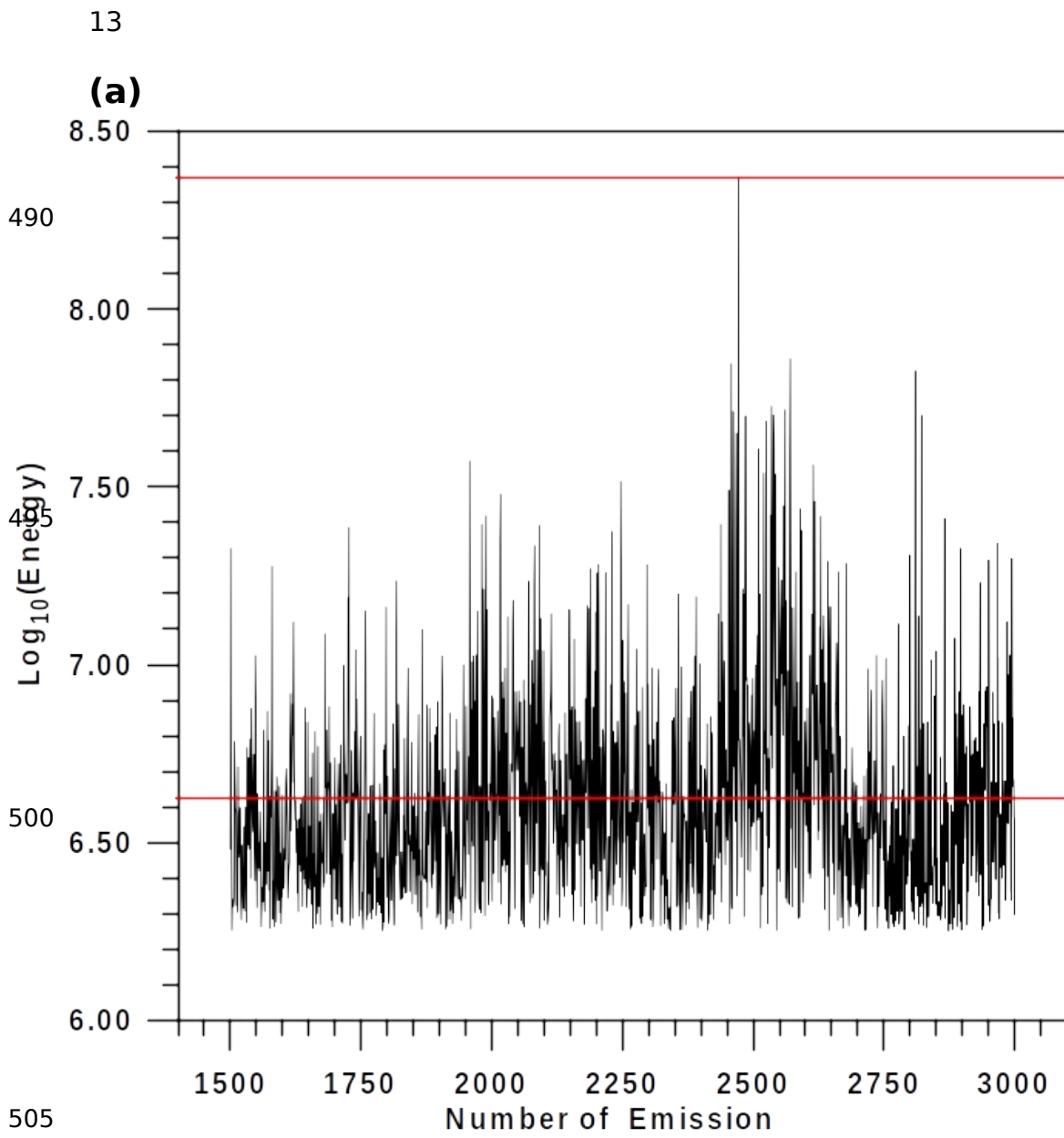
$$\log(N) = -3.84 \log(E) + 33.14$$
$$(\rho^2 = 0.994)$$
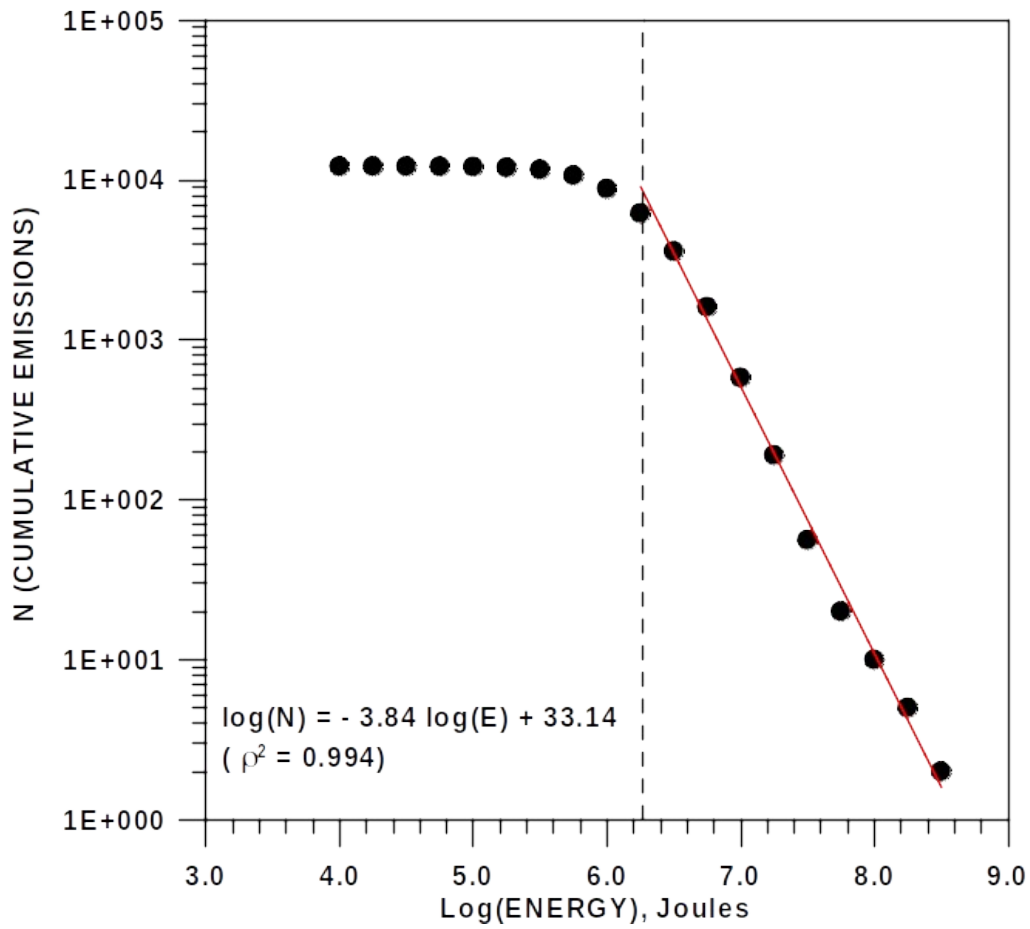
Figure 1. Volcanic energy (Joules) emissions above $\log_{10}(E) = 6.1$ and complying with the Gutenberg-Richter law, as indicated by the red line.

475

480

485

(a)

490

495

500

505

(b)

510

515

520 **Figure 2. a)** The analysed segment of energy emissions by means of multifractal theory, including the highest energy close to $10^{8.4}$ J. The red line indicates the threshold value of Mc completeness magnitude obtained from the Gutenberg-Richter law fit shown in Figure 1. **b)** The same segment of energy distributed along close to 500 consecutive days from 2013/12/10 to 2015/04/24. The largest energetic episode is highlighted with a red line. The red rectangle shows the low activity prior to the major volcanic explosion.

525 **(a)**

(b)

530

535

540

(c)

(d)

(e)

(f)

545

550
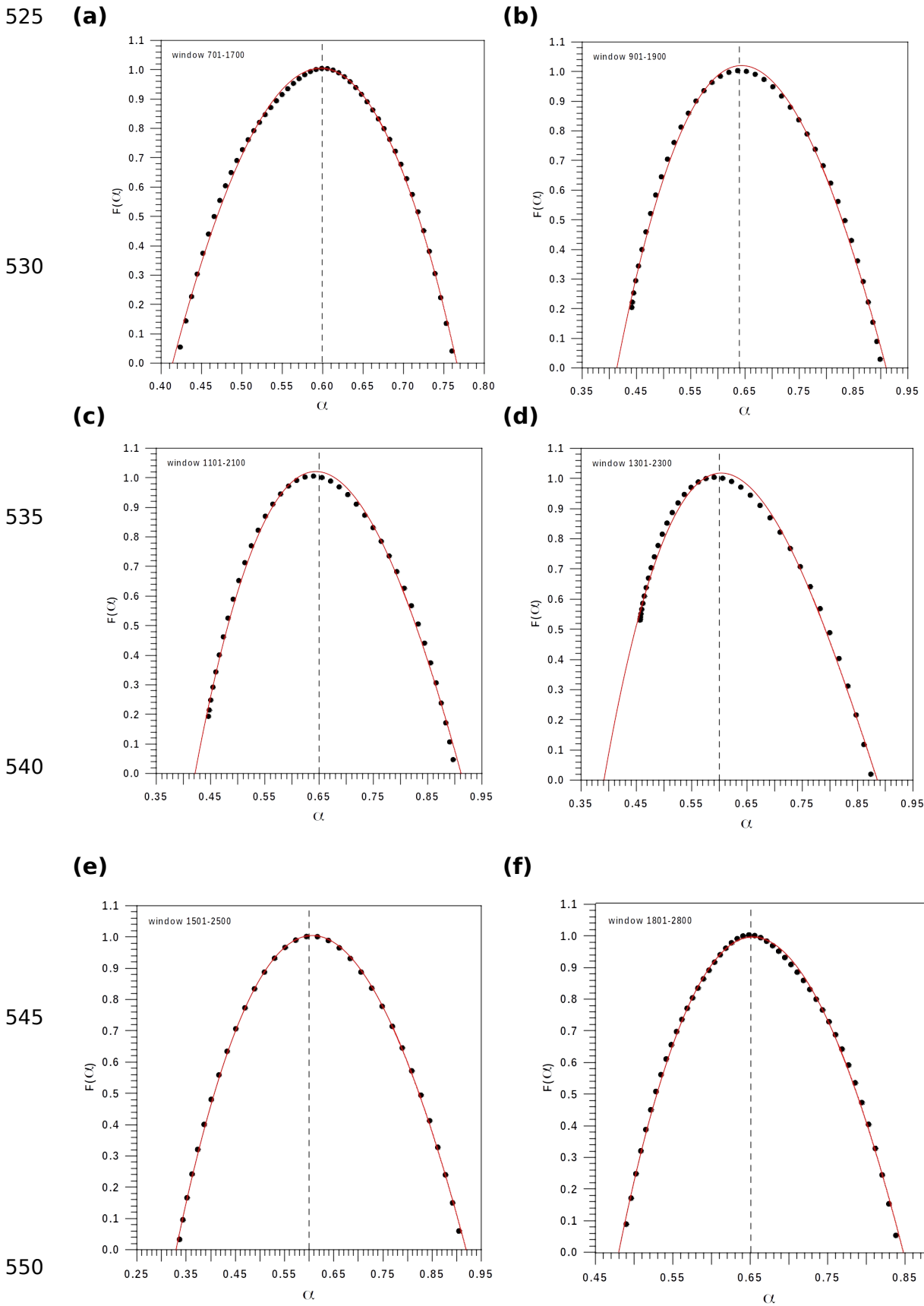
Figure 3. Six examples of multifractal spectrum. (a) – (d) depicts the multifractal spectrum for four moving windows (before the highest emission), (e) and (f) show two last (after the highest emission) moving windows including the extreme energy 555 episode.

(a)

(b)

(c)

(d)
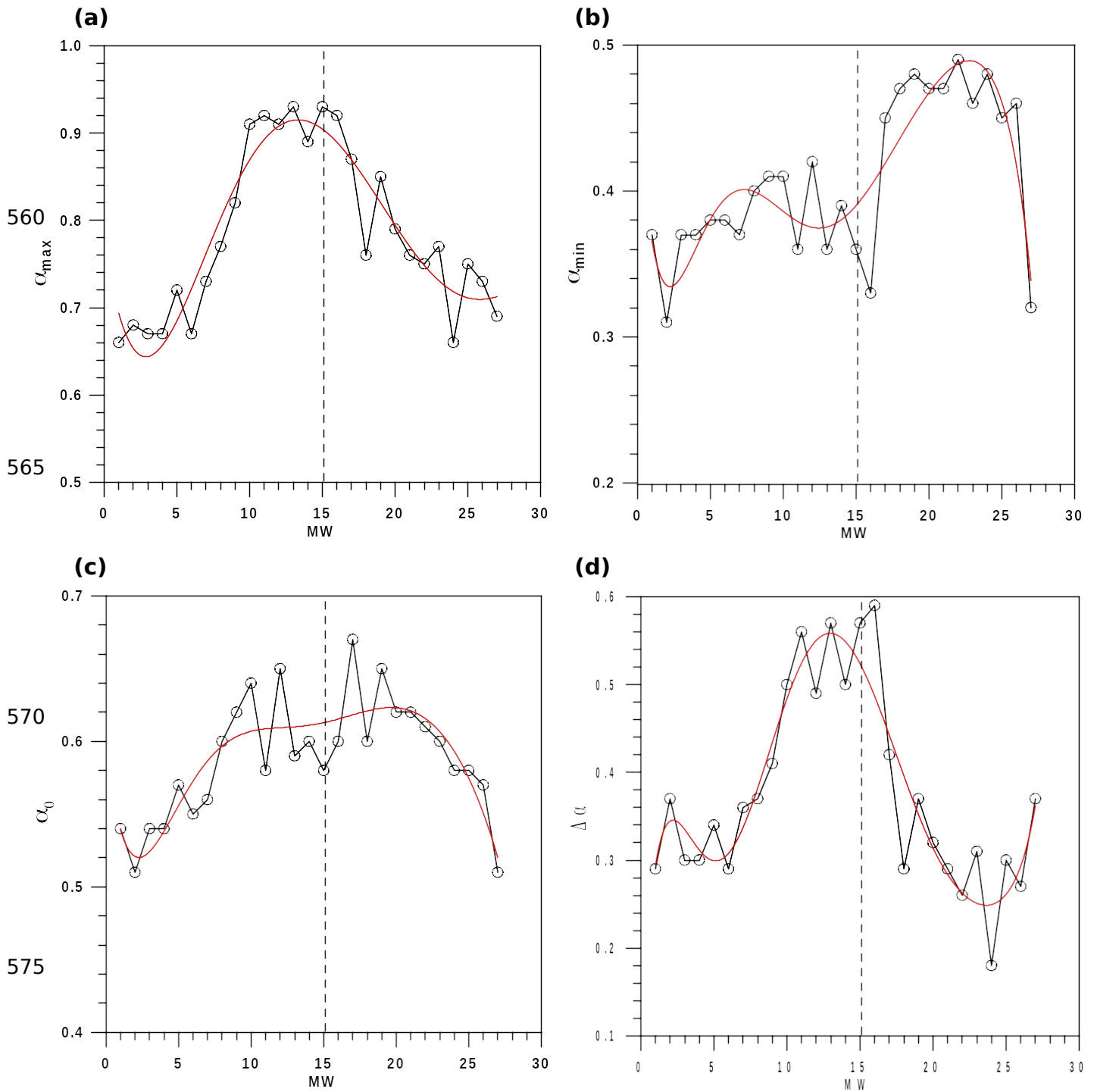
Figure 4. Evolution of the parameters (a) α_{max}, (b) α_{min}, (c) α_0 and (d) $\Delta\alpha$ describing the structure of the multifractality along the 27 moving windows. Red lines describe the smooth evolution of these parameters by means of a polynomial of 5th degree, with a r^2 = 0.88, 0.74, 0.72 and 0.85 respectively. The dashed line indicates MW = 15, which is window the preceding the highest emission.

(a)

(b)

590

595

600

605

610
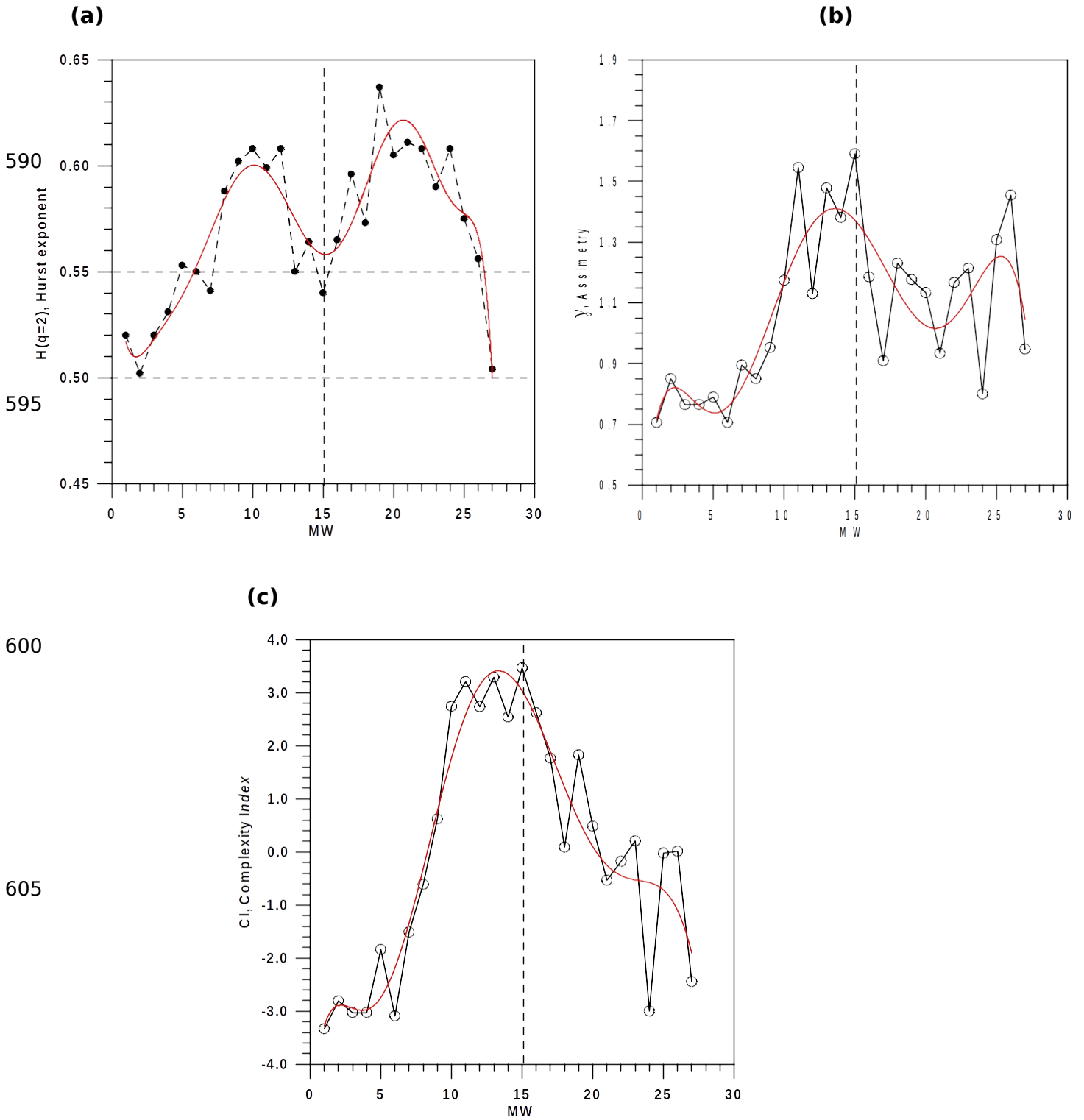
Figure 5. Evolution of a) the Hurst exponent, H(q=2), b) asymmetry, g, and c) complexity index, CI, of the multifractal structure. Red lines describe the smooth evolution of these parameters by means of a 5th degree polynomial with a r^2 = 0.85, 0.68, 0.89 respectively. The dashed line indicates MW = 15, which is the window preceding the highest emission.

615

(a)

(b)

(c)

(d)

(e)

(f)
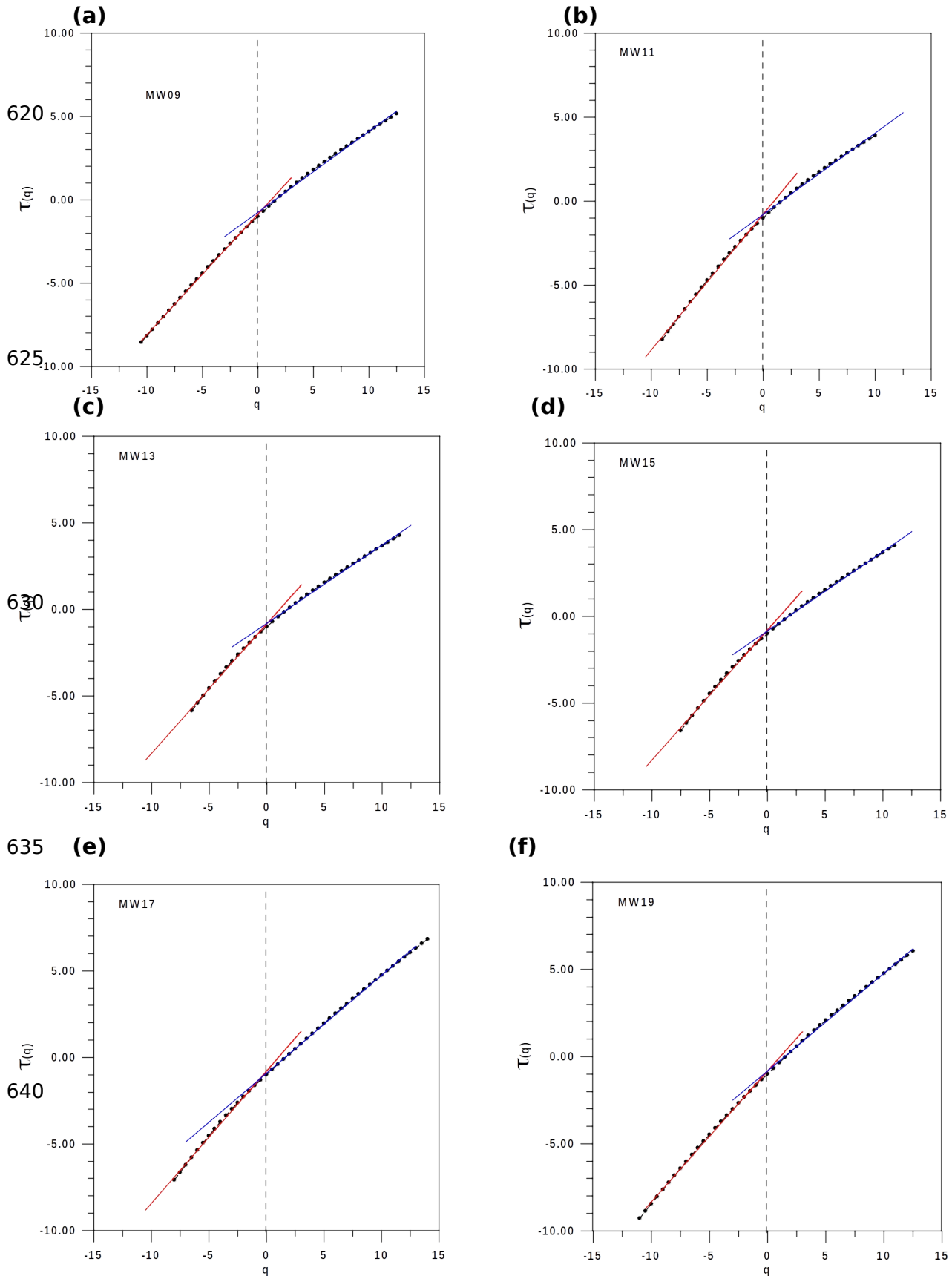
Figure 6. Three examples of $\tau(q)$ for Moving Windows not including the highest emission (a)-(c), and three including the highest energy emission(d)-(f). The change of the $d\tau(q)/dq$ is always detected in $q = 0$ and the corresponding square regression coefficients of both linear evolutions are very close to 1.0
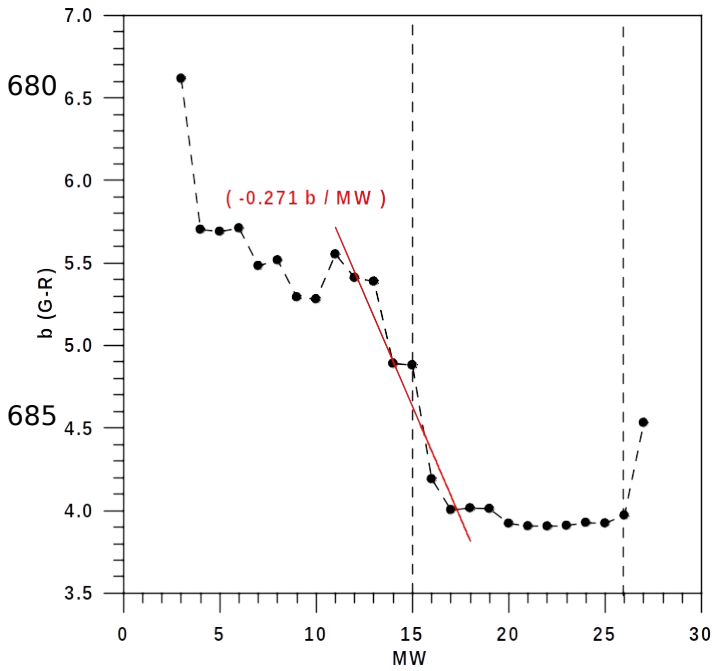
650

655

660
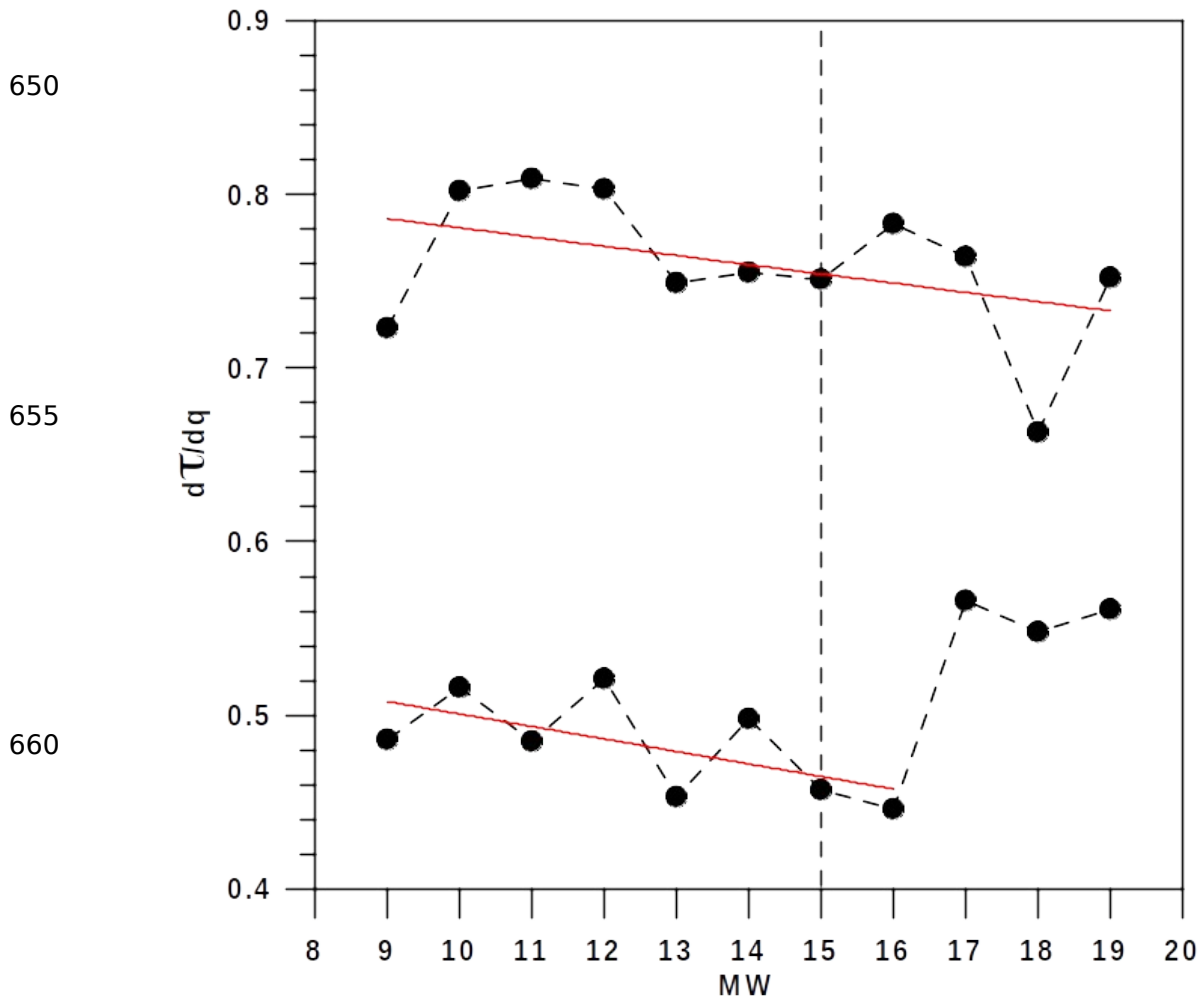
665 **Figure 7**. Evolution of a) dτ/dQ for the moving windows 9 – 19, with the four last MW including the highest emission of energy of figure 1.
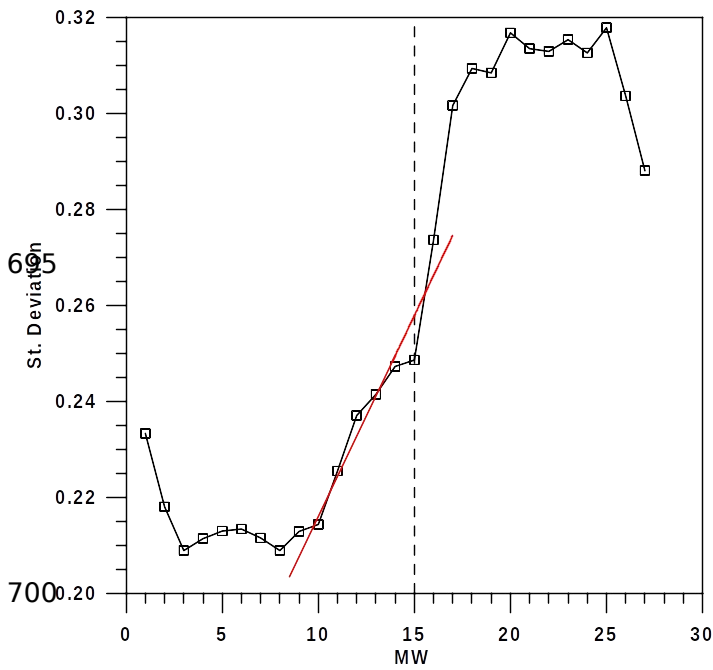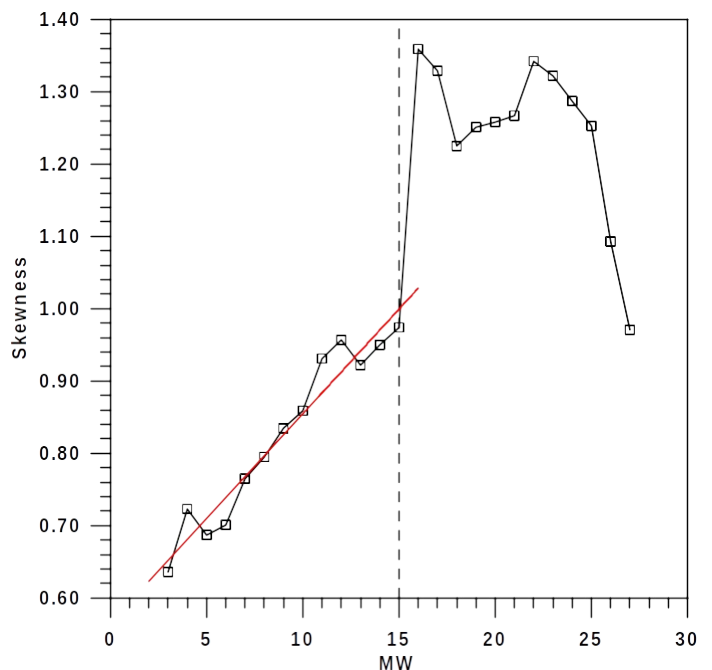
670

675

(a)

(b)

(c)

Figure 8. Statistical values per each moving window, MW: (a) *b*-value, (b) standard deviation and (c) skewness of emission energy E. Red lines represent the linear trends corresponding to MWs close to the extreme emission. Dashed lines show MW = 15 which is the window preceding the highest emission.